2008 American Control Conference
Westin Seattle Hotel, Seattle, Washington, USA
June 11-13, 2008

Ultracapacitor Assisted Powertrains: Modeling, Control, Sizing, and The Impact on Fuel Economy

Dean Rotenberg Ardalan Vahidi Ilya Kolmanovsky

***Abstract*— A mild parallel hybrid powertrain is considered in which an electric motor and an ultracapacitor-based energy source assist the combustion engine during periods of high power demand. The ultracapacitor may be recharged by the engine during periods of low demand, and through regenerative braking. A rule-based control strategy is defined, which determines the power split between the engine and motor. Standard city-cycle simulations on a full-order model of the powertrain illustrate an improvement in fuel economy enabled by the ultracapacitor-based mild hybrid configuration and this control strategy. The deterministic dynamic programming is also applied to the reduced-order model of the powertrain to assess fuel economy potential of the hybrid system under pointwise-in-time and terminal constraints on the state of charge and motor power limits.**

I. Introduction

A vehicle that averages 30 miles per gallon in fuel consumption could have poor instantaneous fuel economy during rapid accelerations. A simple back-of-the-envelope kinetic energy calculation shows that accelerating a 2000 kg vehicle (roughly the size of a Ford Explorer SUV) from 0 to 60 mph (0 to 26.82 m/s) in 10 seconds requires almost 70 kW of power in addition to the power needed to overcome road and air drag forces. Almost the same amount of additional power (70 kW) is needed during a 1 second accelerator pedal tip-in which increases the velocity of the same vehicle from 45 to 48 mph. Situations such as these may consume a disproportionately high amount of fuel, and have a negative impact on the fuel economy of the vehicle. In conventional powertrains, the engine is typically sized larger than needed for steady-state operation, to meet these spikes in power demand.

These situations are believed to be well-suited to the performance characteristics of ultracapacitors, and that the assistance of an electric motor during these periods will allow for a reduction in engine fuel flow rate; further improvements in fuel economy may be possible by downsizing the engine. High power-density ultracapacitors integrated with vehicle powertrains (in a mild parallel hybrid configuration) can boost the power during vehicle acceleration, relax the engine transients and may therefore be an effective mechanism for reducing fuel consumption and emission levels without compromising vehicle agility [1], [2]. Moreover, in many situations, regenerative braking alone may provide sufficient energy for this power boost [3]. The additional cost and weight of the ultracapacitor and electric motor may be justified by a downsized internal combustion engine and, since transients the engine is exposed to are reduced, even possibly a less costly catalytic converter.

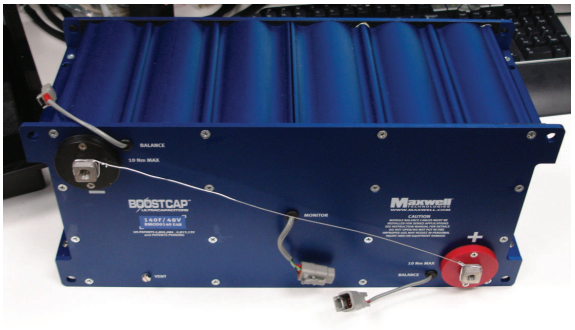

Fig. 1. The 48 volt BMOD0140 Maxwell ultracapacitor module with capacitance of 140F (Dimensions $41.6 \times 19 \times 16$cm, Mass$\approx$ 13.6 kg). While the maximum total energy stored is a mere 161kJ, this energy can be released in just a few seconds generating considerable power boost to a vehicle. The maximum power for this product is 4800W per unit mass or almost 65kW instantaneous maximum power. Newer products listed on Maxwell website [4] have even higher power densities.

Reliable operation of ultracapacitors [5], their high power density and their effective life in the order of one million charge cycles [1], [2] make them an attractive power assisting device. Maxwell Technologies [4], a main provider of ultracapacitors in North America, has been introducing new models over the last few years that have higher power densities and reduced cost (See Figure 1). While full hybrid vehicles, which rely on batteries for power levelling, have reached mass production, the use of ultracapacitors in mild hybrids remains a technology to explore. Most of the existing research on ultracapacitor hybrids is geared towards transit buses where their frequent stop-and-go cycle match the operational characteristics of ultracapacitors [6], [7], [8]. Some researchers have proposed use of ultracapacitors as a supplementary storage device to batteries in hybrid vehicles to help extend the battery life [9], [10], [11]. In fuel-cell powered vehicles, ultracapacitors have been considered as an auxiliary power source which can assist the fuel cell during startup and fast power transients [12], [13], [14], [15]. A concept BMW X3 which was unveiled in 2006, had an ultracapacitor-powered electric motor integrated between the combustion engine and the transmission, helping to boost the engine when accelerating [16].

D. Rotenberg is with The Department of Mechanical Engineering, Clemson University, Clemson, SC 29634 E-mail: drotenb@clemson.edu.

A. Vahidi (corresponding author) is with The Department of Mechanical Engineering, Clemson University, Clemson, SC 29634 E-mail: avahidi@clemson.edu.

I.V. Kolmanovsky is with Ford Research and Advanced Engineering, Ford Motor Company, Dearborn, MI 48124, E-mail: ikolmano@ford.com.

978-1-4244-2079-7/08/$25.00 ©2008 AACC.

The objective of this paper is to assess the extent to which an ultracapacitor, as a stand-alone power assist device, can improve the fuel economy of a mid-size passenger vehicle without sacrificing the vehicle's ability to follow a given velocity profile. As discussed in [17], this kind of assessment for advanced powertrain systems necessitates the synergistic treatment of both design and control issues. A parallel mild hybrid powertrain is considered in which an induction motor powered by an ultracapacitor module assists the combustion engine during acceleration power peaks. The ultracapacitor module is recharged back by the engine during normal cruise or through regenerative braking. A detailed 3-state model of the powertrain is developed to determine via simulation the impact of proposed configuration and the power management scheme on fuel economy and vehicle performance. A representative reduced-order single-state model of the powertrain is also created and is used for the determination of the optimal control of the ultracapacitor with the help of dynamic programming and also for devising a power management strategy. A rule-based power management strategy is developed and its performance is verified on the detailed model in simulation of UDDS city driving cycle.

II. The Hybrid Powertrain Configuration and Models

The ultracapacitor hybrid concept was first evaluated using the PSAT (Powertrain Systems Analysis Toolkit) package [18] in order to ensure that the components, parameter values, and the model are realistic. PSAT, created by Argonne National Laboratory, allows the user to specify a desired powertrain configuration and select pre-existing models of the various powertrain components from an extensive library of production vehicles. The software then assembles the components into a Simulink model, uses a standard control module for power management and simulates the performance over a selection of standard driving cycles.

An existing model of a 2-wheel drive full-size SUV powertrain with a 6 cylinder, 4 liter, 160kW engine was selected as the baseline (conventional) model. An induction motor powered by an ultracapacitor power source was integrated between the combustion engine and the torque converter of the conventional model, to create the ultracapacitor hybrid model. Different size motors were tested with a 93 volt ultracapacitor module with capacitance of 78F. The energy storage capacity of the chosen ultracapacitor module is 93.7 Wh and is consistent with [1], which suggests that "in passenger car applications, for ultracapacitors to compete in terms of cost with batteries, the energy stored should be less than 100 Wh".

Next it was desired to create a simple control algorithm that could be easily tuned and used in fuel economy evaluation of the ultracapacitor-equipped hybrid powertrain. To this end, two new models were created which are based on the PSAT model but operate independently from the PSAT software: 1) a 3-state model was created for simulation of the powertrain; we refer to this as the full-order model, and 2) a reduced single-state model which captures the ultracapacitor's state-of-charge dynamics was developed and is well-suited for the control design; we refer to this model as the reduced-order model.

A. The Full-Order Model

The full-order model is designed to simulate the performance of the powertrain under the demands of standard driving cycles. It contains the vehicle velocity, the torque converter input speed, and ultracapacitor state-of-charge as dynamic states. The full-order model is inspired by the PSAT model and is similar to it in structure; however, the signals are streamlined, some components are simplified and the constraints are managed at the component level.

The effective voltage provided by the ultracapacitor is:

$$V_{out} = V_{oc} - i_{uc}R \tag{1}$$

$$R = \begin{cases} R_{dis} & i > 0 \\ R_{chg} & i < 0 \end{cases}$$

where V_{oc} is the open-circuit voltage of the ultracapacitor, i_{uc} is the current drawn from the ultracapacitor, and R_{chg} and R_{dis} are the line resistances for charging and discharging, respectively. The capacitance C, along with R_{chg} and R_{dis}, are functions of temperature and current determined by maps. These and other maps were obtained using empirical data taken from PSAT [18]. The state-of-charge of the ultracapacitor is defined as:

$$soc = \frac{V_{oc}}{V_{max}} \tag{2}$$

where V_{max} is the maximum open-circuit voltage of the ultracapacitor at full charge. The ultracapacitor charging or discharging current is given by:

$$i_{uc} = \frac{P_{mot}}{\beta V_{out}} \tag{3}$$

where P_{mot} is the motor power. The coefficient β, is:

$$\beta = \begin{cases} \eta_{discharge} & \text{while discharging} \\ 1/\eta_{charge} & \text{while charging} \end{cases} \tag{4}$$

where η_{charge} and $\eta_{discharge}$ represent the efficiency of charging and discharging the ultracapacitor and include the efficiency of the motor and power electronic devices. Combining (1)-(3), i_{uc} can be calculated:

$$i_{uc} = \frac{socV_{max} - \sqrt{(socV_{max})^2 - \frac{4RP_{mot}}{\beta}}}{2R} \tag{5}$$

The full derivation for (6) and (5) can be found in [19], in which it is shown that there are actually two physical solutions for i_{uc}; the solution that corresponds to minimum resistive losses is retained and can be enforced by the motor controller.

The ultracapacitor state-of-charge dynamics are governed by:

$$\frac{dsoc}{dt} = -\frac{i_{uc}}{CV_{max}} = \frac{-socV_{max} + \sqrt{(socV_{max})^2 - \frac{4RP_{mot}}{\beta}}}{2RCV_{max}} \quad (6)$$

The engine fuel consumption rate is a function of the engine torque and the engine speed, and it is obtained from empirical engine maps available in PSAT database. In the proposed configuration both engine and motor are connected together and to the torque converter. The speed of the engine and the motor are the same and equal to the torque converter input speed. The dynamics of the torque converter are characterized by:

$$J\frac{d\omega_{in,tc}}{dt} = T_{in,tc} - T_{loss,tc} \quad (7)$$

$$T_{in,tc} = T_{mot} + T_{eng} \quad (8)$$

where J is the rotational inertia upstream of the torque converter, and $\omega_{in,tc}$ is the shaft speed upstream of the torque converter, equal to the engine and motor speeds. $T_{loss,tc}$ is mapped as a function of $T_{in,tc}$, $\omega_{in,tc}$, and the slip ratio ω_{ratio}, defined as:

$$\omega_{ratio} = \frac{\omega_{out,tc}}{\omega_{in,tc}} \quad (9)$$

where $\omega_{out,tc}$ is the rotational velocity of the powertrain downstream of the torque converter. The torque supplied by the torque converter to the drivetrain is mapped from the slip ratio, and is characterized by:

$$T_{out,tc} = \omega_{in,tc}^2 \times f_1(\omega_{ratio}) \quad (10)$$

where $f_1(\cdot)$ represents a map which is available from PSAT database. The gearbox is modeled as a gear ratio and a loss term. The torque supplied by the gearbox to the downstream components is given by:

$$T_{out,gb} = g_t \times (T_{out,tc} - T_{loss,gb}) \quad (11)$$

where $T_{loss,gb}$ is mapped as:

$$T_{loss,gb} = f_2(\omega_{out,gb}, T_{out,tc}, g_t) \quad (12)$$

and the output speed is determined as:

$$\omega_{out,gb} = \frac{\omega_{out,tc}}{g_t} \quad (13)$$

In this work, we use the gear determined by the PSAT shifting strategy; in future work shifting can be treated as an extra degree of freedom to maximize the fuel economy improvement.

The wheel torque and speed are also influenced by the final drive ratio:

$$T_w = g_f \times T_{out,gb} - T_{loss,fd} \quad (14)$$

$$\omega_w = \frac{\omega_{out,gb}}{g_f} \quad (15)$$

where the final drive ratio g_f, and the loss term $T_{loss,fd}$, are constants.

The vehicle longitudinal dynamics is:

$$M\frac{dv}{dt} = \frac{T_w}{r_w} - F_{grade} - F_{drag} - F_{brake} \quad (16)$$

where M and v are the mass and velocity of the vehicle, r_w is the wheel radius, and F_{grade} is the force due to weight and road grade:

$$F_{grade} = [\sin(\theta) + (\mu_1 + \mu_2\omega_w)\cos(\theta)]Mg$$

where μ_1 and μ_2 are friction coefficients, and θ is the road grade. The aerodynamic drag force is $F_{drag} = Cv^2$, where C is a scaled drag coefficient [20]. Assuming no wheel slip, $v = r_w\omega_w$. The friction brake force at the wheels is represented by F_{brake}.

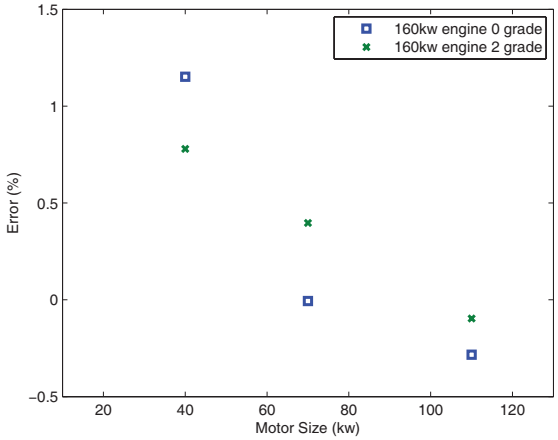

Fig. 2. Percent error in fuel consumption between the original PSAT simulation results and those obtained from the full-order model, applied over the UDDS cycle with no grade and a 2% grade.

The full-order model was tested for consistency against its parent PSAT model by replacing the controller portion of the model with forcing functions developed from PSAT simulation results. The powertrain in the full-order model was thus subjected to the same demands that had been seen by the PSAT powertrain model during various simulations, and its open-loop output was compared with the results of these simulations. Simulations were run for three different combinations of motor sizes: induction motors of 110kW, 70kW, and 40kW were combined with the 160kW engine. The results of this comparison are shown in Figure 2. The relative error of the full-order model is less than 1.2 percent.

B. The Reduced-Order Model

Since the reduction in the number of states helps reduce the complexity of control design, a reduced-order model of the powertrain with only one state, ultracapacitor state-of-charge, has been also created. The state-of-charge dynamics is the same as in the full-order model and represented by equations (6) and (5). However, in the reduced-order model, it is assumed that the line resistance R and capacitance C are independent of internal temperature of the ultracapacitor and are constant. The temperature-dependent changes in the

internal resistance of the ultracapacitor are important [21] and are considered in the full-order model.

The reduced-order model does not contain the entire powertrain. The transmission, torque convertor, and the driver model are external to the reduced-order model and are used to calculate the power demand and engine (and motor) shaft speed which are then fed as inputs to the reduced-order model.

In the reduced-order model, the engine fuel consumption rate and motor efficiencies are modeled algebraically, using the Willan's line method:

$$\dot{m}_f = \frac{aT_{eng}\omega_{eng} + b\omega_{eng} + c\omega_{eng}^3}{\bar{a} + \bar{b}\omega_{eng} + \bar{c}\omega_{eng}^2} \tag{17}$$

$$\eta_{mot} = \frac{e_{mot}T_{mot}\omega_{mot}}{T_{mot}\omega_{mot} + P_{loss,mot}} \tag{18}$$

where ω_{eng}, ω_{mot}, T_{eng}, and T_{mot} are the rotational velocities and output torques of the motor and engine, respectively. η_{mot} is the energy efficiency of the motor, and $\dot{m}_f$ is the mass consumption rate of fuel. The other parameters (e_{mot}, $P_{loss,mot}$, a, b, c, $\bar{a}$, $\bar{b}$, and $\bar{c}$) are determined numerically from performance characteristics of the selected engine and motor available in the PSAT database.

The reduced-order model is used to assess the fuel economy potential of the hybrid powertrain via dynamic programming, as described in the next section.

III. Assessing Fuel Economy Potential Using Dynamic Programming

The fuel economy potential of a powertrain with storage elements (such as an ultracapacitor) and guidelines for operating policy can be assessed using Deterministic Dynamic Programming (DDP) [17]. Computationally, DDP reduces to value function iterations of the form

$$V(x,t) = \min_u \{L(x,u,w(t)) + V(f(x,u,w(t)),t+1)\}, \tag{19}$$

where, assuming the reduced order model, t is the time instant over the drive cycle (sampling interval of 100 msec was used), x is the state (soc), u is the control ($u = s_f$, $P_{mot} = s_f \cdot P_w$ and s_f is referred to as the split fraction), $w(t)$ is the vector of vehicle speed and vehicle power prescribed by the drive cycle, L is the incremental cost function, and the optimal control sequence, $\{u(t)\}$, is a minimizer in (19). The incremental cost L was chosen as a weighted sum of the fuel flow rate and square of motor power. Constraints on state of charge, soc, (specifically, $0.5 \le soc(t) \le 0.9$ and that soc at the end of the drive cycle must be between 0.7 and 0.75) were imposed by augmenting to L, appropriate penalty functions (as per approach in [17]). The control constraints have been defined so that the expression under the square root in (5) is non-negative, thereby guaranteeing that the motor power P_{mot} can be realized by the ultracapacitor, and that $-1 \le s_f \le 1$ if $P_w \ge 0$ and $0 \le s_f \le 1$ if $P_w < 0$. Further a vehicle velocity dependent constraint on minimum and maximum motor power limits has been imposed. We have

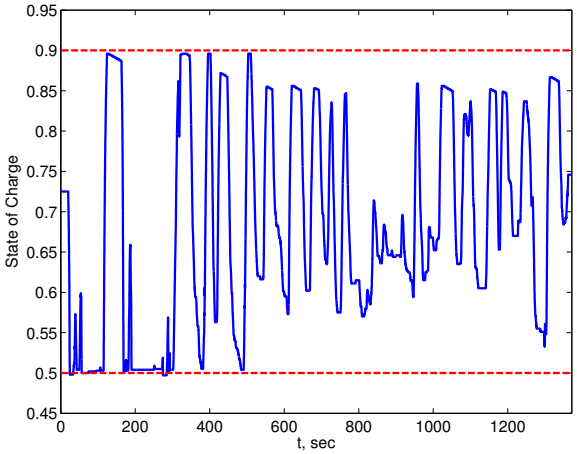

Fig. 3. Trajectory of the ultracapacitor state-of-charge when P_{mot} is optimally controlled, applied over the UDDS driving cycle with no road grade. Pointwise-in-time constraints on *soc* are shown by the dashed lines.

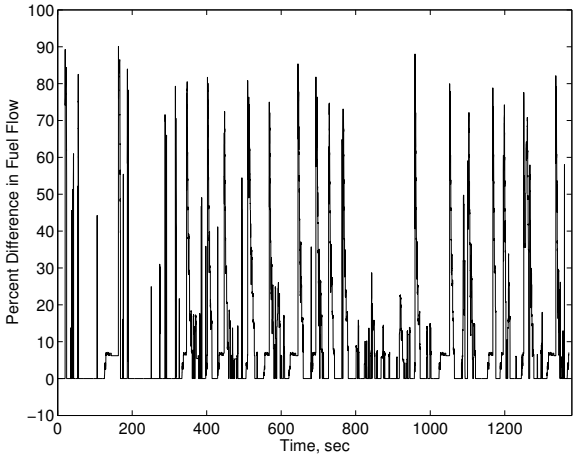

Fig. 4. Percent difference in fuel flow rate between the case when $P_{mot} = 0$ and when P_{mot} is optimally controlled, applied over the UDDS cycle with no road grade.

applied DDP to UDDS profile on 0 degree grade and with a power demand trajectory corresponding to aggressive following of the drive cycle. The vehicle has a 160kW engine and a 110kW maximum-power electric motor. Figures 3 and 4 illustrate the trajectory of soc and the difference in the fuel flow rate between the case when $P_{mot} = 0$ and when P_{mot} is optimally controlled. The fuel consumption difference between these two cases is 15.0% and it provides an estimate for achievable performance when optimization of control as a function of time is performed against a drive cycle known in advance. Figure 3 shows that the constraints on the state of charge are satisfied. From the analysis of optimal trajectories, it has been established that the ultracapacitor is almost exclusively charged from the regenerative braking events. Only a fraction of the full benefit can be attained by an implementable rule-based control strategy, which will be discussed next.

IV. The Rule-Based Supervisory Control Algorithm

With the potential of the ultracapacitors established using the reduced-order model and DDP, a simpler rule-based

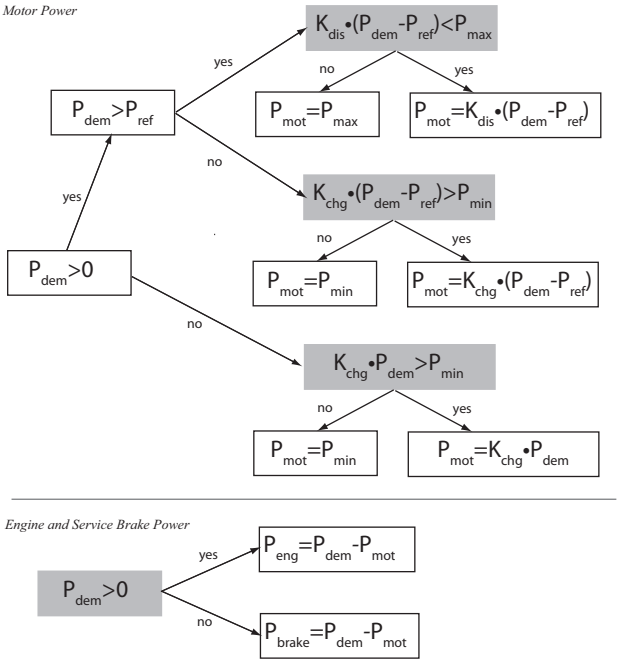

Fig. 5. Flow chart showing the decision tree of the rule-based control algorithm.

power management strategy is designed and employed in closed-loop simulations on the more accurate full-order model. During propulsion, the rule-based algorithm utilizes the motor to assist the engine when the power demanded is higher than a threshold, and to charge the ultracapacitor when it is lower than a threshold, P_{ref}. The state of charge of the ultracapacitor is tracked by the controller, and the maximum allowable power in or out of the motor is reduced as the ultracapacitor nears its minimum or maximum charge of $soc_{max} = 0.9$ and $soc_{min} = 0.5$, respectively. This keeps the motor from switching from high power immediately to no power when the ultracapacitor reaches either limit.

During braking, the motor charges the ultracapacitor, and is subject to the same state of charge restrictions as during propulsion. Friction brakes are assumed to be engaged any time the demanded power falls outside of the motor's lower power limit. The motor is also restricted from charging the ultracapacitor while the engine speed is below the idling speed.

TABLE I

DESCRIPTION OF TERMS USED IN RULE-BASED CONTROL ALGORITHM FLOW CHART.

P_{eng}	Engine Power Demand	P_{max}	Maximum Motor Power
P_{mot}	Motor Power Demand	P_{min}	Minimum Motor Power
P_{brake}	Friction Brake Demand	K_{chg}	Charge Coefficient
P_{dem}	Total Power Demand	K_{dis}	Discharge Coefficient
P_{ref}	Desired Engine Power	soc	State of Charge

$$K_{chg} = \frac{soc_{max} - soc}{soc_{max} - soc_{min}} \tag{20}$$

$$K_{dis} = \frac{soc - soc_{min}}{soc_{max} - soc_{min}} \tag{21}$$

A graphic representation of the rule-based control algorithm is given in Figure 5, with the terms used described in Table I and in the accompanying equations (20) and (21).

V. RESULTS USING THE RULE-BASED POWER MANAGEMENT STRATEGY

The fuel economy was evaluated by simulating the full-order model controlled by the rule-based strategy over various driving cycles. Shown in Figures 6, 7, and 8 is time history of several of the performance characteristics of the powertrain over the UDDS cycle with no road grade, using the 160kW engine and a 110kW electric motor. This simulation showed a fuel economy improvement of slightly more than 11% over the conventional powertrain.

For this cycle, it appears that a smaller motor and engine would be sufficient. For the majority of the cycle, the ultracapacitor is able to meet its demands without reaching the charge limits imposed upon it. The results also indicate that the energy provided by regenerative braking is more than sufficient to sustain the motor's assistance to propulsion for these driving conditions, and that motor is only utilizing a portion of the available braking energy.

Next, to determine the effect of component sizing, the performance of different sizes of motor and ultracapacitor were simulated with the full-order model and rule-based controller. Induction motors with maximum power of 110kW, 70kW, and 40kW were combined with three sizes of ultracapacitors. Tables II and III summarize the components used.

The fuel economy of each case was compared to that of the conventional vehicle in full-order model simulations. Figures 9 and 10 summarize the fuel economy improvement for UDDS cycle tests applied over 0 and 2 percent road grades, respectively. The hybrid powertrains were able to produce the results shown while being able to follow the desired vehicle velocity profile. Velocity plots are not shown, because the velocity profiles are indistinguishable from those of the conventional case. As seen in these Figures, the smaller 40kW motor has the best fuel economy results and therefore is a better choice over the originally chosen 110kW motor, most probably due to the reduced weight and more efficient operation of the smaller motor. On a flat road (zero percent grade) the larger ultracapacitor modules result in better fuel economy than the 93V 78F ultracapacitor, but on a 2-percent grade road the advantage of larger ultracapacitor sizes seem to diminish. On the same note, the largest ultracapacitor does not always yield the best fuel economy; this may be due to the added weight and a particular combination of components. Moreover the larger sizes (> 100Wh) may not be an economically viable alternative to batteries according to [1]. Therefore the 93V 78F ultracapacitors seems to be the best trade-off among the three ultracapacitors compared.

To investigate the expected benefits of downsizing the combustion engine in the ultracapacitor assisted powertrain, we ran a number of tests with a smaller 120kW engine

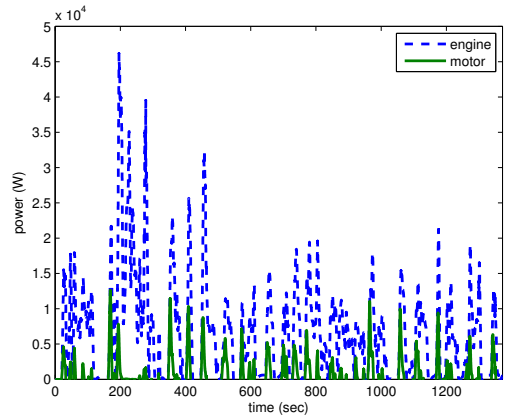

Fig. 6. Time history of power provided by the motor and the engine during propulsion of the vehicle over UDDS cycle with zero percent road grade, using a 160kW engine and 110kW motor.

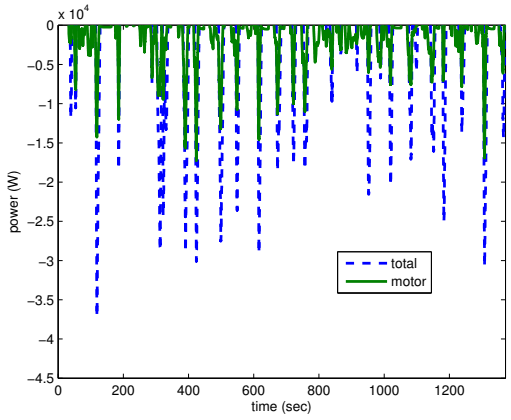

Fig. 7. Time history of power provided by the motor and the friction brakes during braking of the vehicle over UDDS cycle with zero percent road grade, using a 160kW engine and 110kW motor.

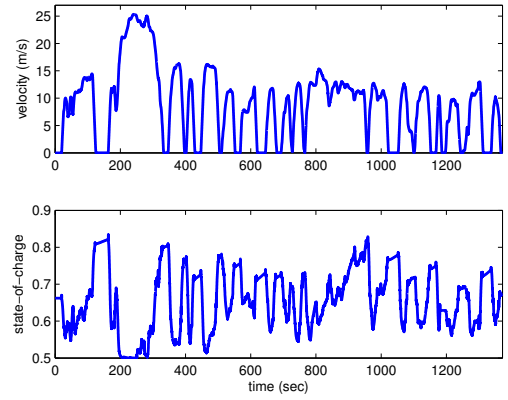

Fig. 8. Time history of vehicle velocity and ultracapacitor state-of-charge over UDDS cycle with zero percent road grade, using a 160kW engine and 110kW motor.

chosen from the PSAT database. Table IV shows the fuel economy improvement over the conventional powertrain for the 120kW and 160kW engines (both with the 40kW motor and the 93V, 78F Ultracapacitor). The vehicle with the downsized 120kW engine was able to follow the UDDS cycle on both 0 and 2 percent grades and the fuel economy was

TABLE II

DIFFERENT MOTOR SIZES TESTED.

Max. Power (kW)	Continuous Power (kW)	Weight (Kg)
40	21	30
70	35	115
110	75	92

TABLE III

DIFFERENT ULTRACAPACITOR SIZES TESTED.

Voltage (V)	Cap (F)	Energy (Wh)	Weight (Kg)
93	78	93.7	35.46
93	156	187.4	70.92
93	234	281.1	106.38

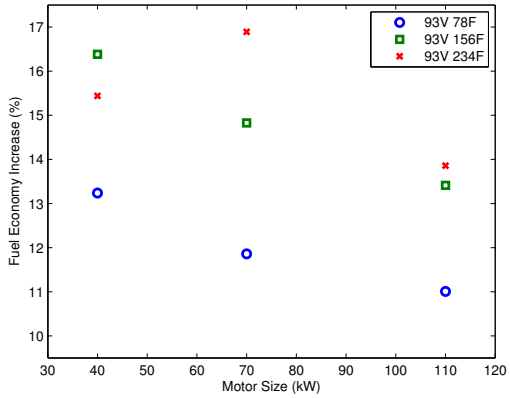

Fig. 9. Percent increase in fuel economy between conventional powertrain and hybrid powertrain with various motor and ultracapacitor sizes, applied ove

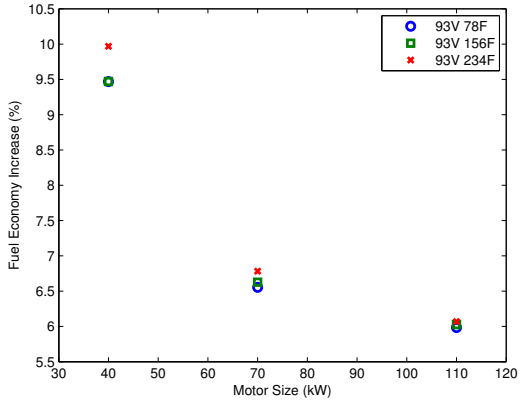

Fig. 10. Percent increase in fuel economy between conventional powertrain and hybrid powertrain with various component sizes, applied over the full-order model with UDDS driving cycle and a 2% road grade.

better than the conventional powertrain. On zero percent grade the 120kW engine consumed less fuel than the hybrid with 160kW engine, but on the 2 percent grade this was reversed. This may be due to several factors, 1) the smaller engine having to overwork on the 2 percent grade, 2) the limitations of the rule-based algorithm and its sensitivity to its choice of parameters 3) the gear shifting strategy which is not optimized for the mild hybrid powertrain. These observations call for a more detailed analysis of engine downsizing based on more case studies, and application of dynamic programming which is planned for future work.

TABLE IV

PERCENT FUEL ECONOMY IMPROVEMENT WITH DIFFERENT ENGINES.(UDDS CYCLE, 40KW MOTOR, 93V, 78F UC)

	0% grade	2% grade
120kW engine	+14.4%	+7.4%
160kW engine	+13.2%	+9.5%

VI. CONCLUSIONS

A mild ultracapacitor hybrid powertrain concept considered in this paper shows a potential to improve the fuel economy of passenger vehicles in city driving. The potential for improvement was first assessed in simulations on a reduced-order vehicle model and with optimal power split strategy determined by deterministic dynamic programming. The improvement was further assessed using a more accurate full-order model simulations, together with a real-time-implementable rule-based power split scheme. Results also indicate that the energy provided by regenerative braking may be sufficient to sustain the motor's assistance to propulsion for city driving conditions similar to those encountered in the drive cycle.

This paper has not explored additional fuel economy improvements due to an optimized shifting strategy, nor the improvements possible by implementing a real-time optimization-based control strategy. More detailed analysis is also needed to determine if fuel consumption can be further reduced for a downsized engine or by elimination of the torque convertor. These topics are relegated to future work.

VII. ACKNOWLEDGEMENTS

This research is supported in part by an exploratory research grant from Ford Research and Advanced Engineering. The authors wish to thank Professor John Wagner of Clemson University for his valuable inputs on the project, and Dr. Franco Leonardi and Dr. Mark Jennings of Ford Motor Company for valuable discussions.

REFERENCES

[1] A. Burke, "Batteries and ultracapacitors for electric, hybrid, and fuel cell vehicles," *Proceedings of the IEEE*, vol. 95, pp. 806–820, 2007.

[2] G. Zurpette, "Supercharged," *IEEE Spectrum*, pp. 32–37, 2005.

[3] Z. Juda, "Ultracapacitors as an advanced energy source for braking energy recovery in electric vehicles," *Environment Protection Engineering*, vol. 32, pp. 195–202, 2006.

[4] "http://www.maxwell.com," .

[5] B. Maher, "Ultracapacitors: The battery-less, high reliability back-up solution," *Proceedings of IEEE Twenty-Seventh International Telecommunication Conference*, 2005.

[6] M. Furubayashi, Y. Ushio, E. Okumura, T. Takeda, D. Andou, and H. Shibya, "Application of high power super capacitors to an idling stop system for city buses," *Proceedings of the 18th International Electric, Fuel Cell and Hybrid Vehicles Symposium*, 2001.

[7] J. Major, "Hybrid shuttle bus using ultracapacitors," *Proceedings of Electrical Insulation Conference and Electrical Manufacturing Expo*, pp. 275–278, 2005.

[8] J. Anstrom, B. Zile, K. Smith, H. Hofmann, and A. Battra, "Simulation and field-testing of hybrid ultra-capacitor/battery energy storage systems for electric and hybrid-electric transit vehicles," *Proceedings of IEEE Applied Power Electronics Conference and Exposition*, pp. 491–497, 2005.

[9] A. Stienecker, T. Stuart, and C. Ashtiani, "A combined ultracapacitor - lead acid battery energy storage system for mild hybrid electric vehicles," *Proceedings of IEEE Vehicle Power and Propulsion Conference*, pp. 1599–1604, 2005.

[10] A. Stienecker, T. Stuart, and C. Ashtiani, "An ultracapacitor circuit for reducing sulfation in lead acid batteries for mild hybrid electric vehicles," *Journal of Power Sources*, vol. 156, no. 2, pp. 755–762, 2006.

[11] L. Rosario and P. Luk, "Implementation of a modular power and energy management structure for battery-ultracapacitor powered electric vehicles," *Proceedings of IET Hybrid Vehicle Conference*, pp. 141–156, 2006.

[12] P. Rodatz, O. Garcia, L. Guzzella, F. Buchi, M. Bartschi, A. Tsukada, P. Dietrich, R. Kotz, G. Scherer, and A. Wokaun, "Performance and operational characteristics of a hybrid vehicle powered by fuel cells and supercapacitors," *SAE Paper 2003-01- 0418*, 2003.

[13] R. Kotz, S. Muller, M. Bartschi, B. Schnyder, P. Dietrich, F. Buchi, A. Tsukada, G. Scherer, P. Rodatz adn O. Garcia, P. Barrade, V. Hermann, and R. Gallay, "Supercapacitors for peak-power demand in fuel cell driven cars," *Electrochemical Society Proceedings*, vol. 21, pp. 564–575, 2001.

[14] A. Vahidi, A. Stefanopoulou, and H. Peng, "Current management in a hybrid fuel cell power system: A model predictive control approach," *IEEE Transactions on Control Systems Technology*, vol. 14, pp. 1047–1057, 2006.

[15] P. Rodatz, G. Paganelli, A. Sciarretta, and L. Guzzella, "Optimal power management of an experimental fuel cell supercapacitor-powered hybrid vehicle," *Control Engineering Practice*, vol. 13, pp. 41–53, 2005.

[16] "The BMW concept X3 Efficient Dynamics," Video at http://vodcast.bmw.com/stories/1424704/.

[17] I. Kolmanovsky, S. Sivashankar, and J. Sun, "Optimal control-based powertrain feasibility assessment: A software implementation perspective," in *Proceedings of 2005 American Control Conference*, Portland, Oregon, June 8-10 2005, pp. 4452–4457.

[18] Argonne National Laboratory, "Powertrain system analysis toolkit," commercial software.

[19] A. Vahidi and W. Greenwell, "A decentralized model predictive control approach to power management of a fuel cell-ultracapacitor hybrid," *Proceedings of the American Control Conference*, pp. 5431–5437, 2007.

[20] T.D. Gillespie, *Fundamentals of Vehicle Dynamics*, SAE International, 1992.

[21] W. Lajnef, J.-M. Vinassaa, O. Briata, S. Azzopardia, and E. Woirgarda, "Characterization methods and modelling of ultracapacitors for use as peak power sources," *Journal of Power Sources*, vol. 168, no. 2, pp. 553–560, 2007.